Chaotic dynamics of particle dispersion in fluids

L. P. Wang and M. R. Maxey
Center for Fluid Mechanics, Turbulence, and Computation, Brown University, Providence, Rhode Island 02912

T. D. Burton and D. E. Stock
Department of Mechanical and Materials Engineering, Washington State University, Pullman, Washington 99164

(Received 7 January 1992; accepted 16 April 1992)

An analysis of the Lagrangian motion for small particles denser than surrounding fluid in a two-dimensional steady cellular flow is presented. The Stokes drag, fluid acceleration, and added mass effect are included in the particle equation of motion. Although the fluid motion is regular, the particle motion can be either chaotic or regular depending on the Stokes number and density ratio. The implications of chaotic motion to particle mixing and dispersion are discussed. Chaotic orbits lead to the dispersion of particle clouds which has many of the features of turbulent dispersion. The mixing process of particles is greatly enhanced since the chaotic advection has the property of ergodicity. However, a high dispersion rate was found to be correlated with low fractal dimension and low mixing efficiency. A similar correlation between dispersion and mixing was found for particles convected by a plane shear mixing layer.

I. INTRODUCTION

Chaotic dynamics is now recognized as a common foundation of understanding nonlinear systems. In a specified Eulerian flow field, the response of Lagrangian fluid elements which simply move with the local fluid velocity is described by a set of nonlinear ordinary differential equations, i.e., a dynamical system. Therefore, the methods of chaotic dynamics can be applied to study the Lagrangian fluid motion. Even for simple laminar flows, the resulting dynamical system is nonintegrable and often displays chaotic behavior. This has led to the study of *chaotic advection* or *Lagrangian turbulence*.[1,2] This finding has important implications for fluid mixing and dispersion. A systematic account of fluid mixing by chaotic advection can be found in the book by Ottino.[3]

The idea of chaos has recently been extended to the study of the motion of *foreign* passive particles in moving fluids, e.g., dense particles or droplets in air. These particles follow different trajectories than fluid elements because of the additional effects of inertia and external forces. Consequently the dynamical system has higher dimensionality and allows for richer, and possibly chaotic behavior. The dynamical system that describes the motion of nonzero inertia particles in an incompressible flow is dissipative and as such stable regular attractors or strange attractors may exist. As noted in a review paper by Maxey,[4] it appears to be a common feature that weak or moderate inertial effects over a long period of time lead to very organized regular or periodic particle trajectories. Chaotic orbits that we will be mainly interested in are usually associated with strong particle inertia. In a closely related work, Crisanti *et al.*[5] quantitatively studied the Lagrangian motion of particles in a steady two-dimensional cellular flow where the motion of fluid elements is completely integrable and regular. For particles slightly heavier than the fluid but with strong inertia they found that the particle motion is chaotic and can be characterized by a positive largest Lyapunov exponent. They also showed that a dispersion coefficient can be used to quantify the Lagrangian motion of particle clouds for some parameter ranges. Using numerical simulations they found a similarity between the particle motion and the motion of fluid elements in the presence of molecular diffusion. In other words, strong particle inertia may induce chaotic motion and dispersionlike phenomenon in simple regular flows. This finding seems to add an additional domain to our usual belief that the dispersion processes are only found in complex Eulerian flows, i.e., turbulent fluid flows. For the same cellular flow, Mallier and Maxey[6] found that the settling motion of a nonspherical particle with large aspect ratio is chaotic even in the absence of particle inertia.

A three-dimensional version of this cellular flow is the Arnold–Beltrami–Childress (ABC) flow. The motion of fluid elements in ABC flow is known to be chaotic in the neighborhood of the heteroclinic lines connecting the unstable fixed points.[2] McLaughlin[7] investigated the motion of passive particles in this flow in the limit of very small particle inertia and showed qualitatively that chaotic particle trajectories existed but the degree of chaos tended to be reduced by the particle inertia and virtual mass. Wang *et al.*[8] extended the work by using a wider range of the particle parameters and quantified the Lagrangian motion using fractal dimension. They found that both small and large particle inertia, compared to flow characteristic time scale, eliminated chaos, but for intermediate particle inertia the Lagrangian motion was chaotic and the irregularity was stronger than for fluid elements. Particle settling was shown to reduce chaos and eventually produce periodic or quasiperiodic motion at large settling velocities. Wang *et al.* also attempted to compute the effective particle diffusivity based on a single particle trajectory ignoring the difference in spatial directions. Given the way diffusivity was

 0899-8213/92/081789-16$04.00

computed and the spatial complexity of the ABC flow, no relation between diffusivity and fractal dimension was found.

Some preliminary effort has been made to study Lagrangian motion of particles in fully turbulent flows and shear mixing layers using dynamical systems tools. Wang *et al.*[9] used a finite number of random Fourier modes to represent unsteady, three-dimensional turbulent flow and computed the fractal dimension for the attractor of heavy particles. They found that the fractal dimension increased linearly with increasing particle diffusivity for a wide range of particle inertia and settling velocities. This suggests that the notion of chaos may be useful for studying particle dispersion and mixing in real turbulence. Gañán-Calvo and Lasheras[10] used a steady Stuart vortex solution of the Eulerian equations to represent a plane, free-shear layer and showed that heavy particles can be suspended in the layer and have periodic, quasiperiodic, or chaotic orbits. When the motion is chaotic, the attractor in physical space has a finite height, indicating some degree of transverse dispersion.

Most of the above studies are still of a preliminary nature. They raise many issues that need further, detailed investigation. Questions that come to mind include the following: Why does the appearance of chaos give rise to dispersion? Does the occurrence of chaos guarantee dispersion? What measure based on chaotic dynamics is correlated to the dispersion coefficient? In this paper we address these issues by examining the Lagrangian motion of small, heavy particles in the steady two-dimensional cellular flow. Chaotic orbits are shown to exist and the resulting dispersion of particle clouds are found to have many of the features of turbulent dispersion. Correlations between the fractal dimension, the effective dispersion rate, and the effective mixing efficiency are explored. Finally particle dispersion and mixing in an evolving free-shear layer is briefly discussed in a similar context.

II. AEROSOL PARTICLES IN A CELLULAR FLOW

In this section we examine the Lagrangian motion of aerosol particles in a cellular flow. Such a flow arises in thermal convection with free-slip boundaries and has also been used to represent the transport effects of small-scale turbulent eddies on a passive scalar field.[11] Although the same flow was considered by Crisanti *et al.*,[5] the equation of motion for particles adopted here is more general than in their work and a different particle parameter range is considered. Maxey and his co-workers, in a series of papers,[4,6,12,13] have studied the motion of small spherical and nonspherical particles in the same flow. Their main focus was on particle suspension and possible change in the particle mean settling rate. Our focus is on the chaotic motion of small spherical particles and the relationship between chaos, dispersion, and mixing.

A. Dynamical system

The steady, two-dimensional, and incompressible cellular flow is given in terms of streamfunction ψ in fixed coordinates by

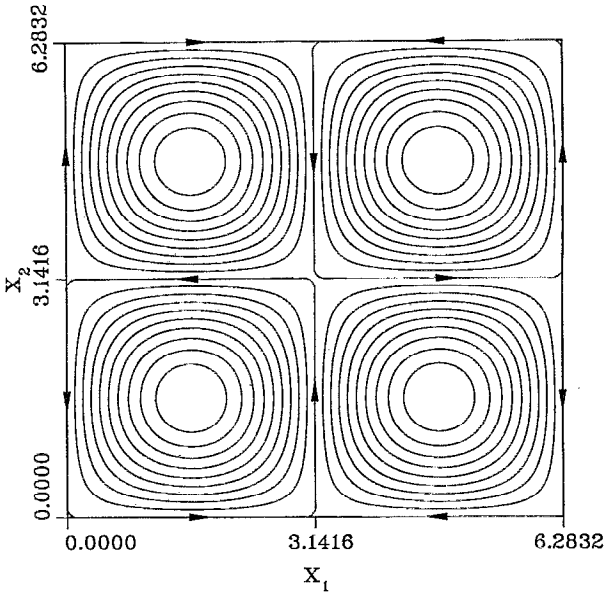

FIG. 1. Streamlines in the cellular flow field. The increment in the values of streamfunction is 0.1.

$$\psi=\sin x_1 \sin x_2. \tag{1}$$

All the variables are assumed to be normalized by a characteristic length scale L and a velocity scale U_0 of the flow.[12] Typical streamlines are shown in Fig. 1. The flow extends with periodic repetition in both the x_1 and x_2 directions. The maximum flow velocity occurs on the cell boundaries, and there are stagnation points at the center of each cell and at the corners. The orbits for fluid elements are streamlines, thus the fluid motion for almost all initial conditions is periodic and regular with a period changing from 2π near the center to infinity near cell boundaries. Equation (1) is a solution to the inviscid Euler equation for steady flow. The pressure is minimum at the center of the cell and maximum at the corners. The pressure gradient provides the force for the rotational motion of the fluid.

We restrict our study to small spherical particles in the aerosol range as defined by Maxey,[12] that is, the ratio of the particle density to the fluid density is larger than 2, $\rho_p/\rho_f > 2$. The particle equation of motion in a steady flow is given in a nondimensional form by[12]

$$\frac{d\mathbf{v}}{dt}=\frac{\mathbf{u}[\mathbf{y}(t),t]-\mathbf{v}}{\mathrm{St}}+R\mathbf{u}\cdot\nabla\mathbf{u}+\frac{1}{2}R\mathbf{v}\cdot\nabla\mathbf{u}. \tag{2}$$

In these equations, $\mathbf{v}(t)$ and $\mathbf{y}(t)$ are particle velocity and location; $\mathbf{u}(\mathbf{x},t)$ is Eulerian flow velocity field, and, for the cellular flow, it is independent of t. The terms on the right-hand side of Eq. (2) represent Stokes drag, the pressure gradient force on the particle (more generally, the fluid force on an equivalent element from the undisturbed flow field), and the added mass effect. The effect of gravitational settling is not considered in the present paper. (One may assume that gravity is aligned in the direction normal to the two-dimensional plane and thus does not affect the motion in the plane.) Equation (2) is a simplified version

of the more general equation of motion.[12] A Stokes drag is assumed here. Previous experience indicates that Stokes drag gives qualitatively similar results as some nonlinear empirical drag law.[14,15] While Eq. (2) may not capture all the relevant physical processes the results of this study should still be representative of those arising in more complicated systems. Two governing parameters appearing in Eq. (2) are defined as

$$\mathrm{St}=\frac{\tau_a U_0}{L}, \quad R=\frac{\rho_f}{\rho_p+\frac{1}{2}\rho_f}, \tag{3}$$

which measure the relative importance of particle inertia and fluid acceleration; τ_a is the particle inertia response time and given by

$$\tau_a=(m_p+\tfrac{1}{2}m_f)/3\pi\, d\mu. \tag{4}$$

Substituting Eq. (1) into Eq. (2) we obtain the dynamical system for the motion of an aerosol particle in the cellular flow:

$$\frac{dv_1}{dt}=\frac{\sin y_1 \cos y_2 - v_1}{\mathrm{St}}+R\sin y_1 \cos y_1 + \tfrac{1}{2}R(v_1 \cos y_1 \cos y_2 - v_2 \sin y_1 \sin y_2), \tag{5a}$$

$$\frac{dv_2}{dt}=\frac{-\cos y_1 \sin y_2 - v_2}{\mathrm{St}}+R\sin y_2 \cos y_2 + \tfrac{1}{2}R(v_1 \sin y_1 \sin y_2 - v_2 \cos y_1 \cos y_2), \tag{5b}$$

$$\frac{dy_1}{dt}=v_1, \tag{5c}$$

$$\frac{dy_2}{dt}=v_2. \tag{5d}$$

This is a four-dimensional nonlinear system in the phase space (v_1, v_2, y_1, y_2). Since the flow is steady the system is autonomous. The volume expansion rate in phase space is given by

$$\frac{\partial \dot{v}_1}{\partial v_1}+\frac{\partial \dot{v}_2}{\partial v_2}+\frac{\partial \dot{y}_1}{\partial y_1}+\frac{\partial \dot{y}_2}{\partial y_2}=-\frac{2}{\mathrm{St}} \tag{6}$$

and is a negative constant. Therefore the system is dissipative and chaotic attractors (of zero volume) may exist. In fact, observing the similarity of power spectrum between the velocity space (v_1, v_2) and the physical space (y_1, y_2) as implied by Eqs. (5c) and (5d), we may assert that the particle clouds in physical space will also take a fractal set at long time. We notice, however, $v_1(t)$ and $v_2(t)$ are stationary in time under most conditions but $y_1(t)$ and $y_2(t)$ are not. The value of $y_1(t)$ and $y_2(t)$ may increase without an upper bound. The fixed points for the system and their stabilities have been discussed in detail by Maxey.[12] In short, fixed points exist on the cell boundaries or at the center of each cell but all of them are unstable.

To specify the motion of a particle, we need initial conditions for the system. The particle initial velocity was set to be zero. Although we cannot exclude the possibility that other initial conditions may give rise to a different long-time solution for a given set of parameters (St, R), test computations did show that the long-time particle motion was not sensitive to the choice of initial particle velocity or location. This will be discussed later in the next section. The system [(5a)–(5d)] is not directly integrable and therefore was solved numerically by a fourth-order Adams method and a fourth-order Runge–Kutta method.[16] A time step of 0.01 was used. Numerical tests showed that average quantities such as Lyapunov exponents were independent of time step for time steps smaller than 0.01. A more stringent test was to numerically integrate the trajectory of a fluid element; it was found that a closed orbit (streamline) was recovered after a long time of integration without any noticeable error. For example, a fluid orbit originating from (1.6, 0.3) was solved for one million time steps with step size 0.01. The period was found to be about 10.6 time units, therefore, the total integration time (10 000) represents about 1000 cycles. Figure 2(a) shows the positions of the fluid element for the first 100 time units, i.e., $t=0,1,2,\ldots,99$; and Fig. 2(b) shows the positions of the fluid element for the last 100 time units starting from $t=9901$. The positions of the fluid elements at all 10 000 time units are plotted in Fig. 2(c). A single closed orbit for such a long time indicates the integration scheme was very accurate, i.e., there was no numerically induced inertia. One should not assume, however, that this implies an *exact* trajectory can be obtained in any case. In fact, if the motion of a particle is chaotic, a computer solution seldom gives the *exact* trajectory because of the exponential amplification of uncertainty by the system itself. In such a case, the integration scheme is viewed to be accurate if further refinement does not alter the overall average features of the trajectory.

It is useful to point out the overall, relative role of the various terms in Eq. (2) on the motion of an aerosol particle in the cellular flow. In the numerical simulations the added mass term was found to be much smaller than the other two terms. Therefore, the main forces on the particle are the drag force and the pressure gradient force. Roughly speaking, the particle inertia represented by the drag force produces a centrifugal effect which causes the particle to move away from the cell center where the vorticity is the strongest. The pressure gradient force has an opposite effect on the motion of the particle, i.e., pushing the particle back to the center of the cell. The two competing effects are controlled by the product, $\mathrm{St}\cdot R$, e.g., if $\mathrm{St}\cdot R>1$, the pressure gradient force dominates over the drag force. For this reason, the value of $\mathrm{St}\cdot R$ should play an important role in our system.

B. Periodic and chaotic orbits

For various combinations of St and R, the particle orbits were found to be either chaotic or periodic. The boundary curve between chaotic and periodic motion in the parameter space (St, R) is shown in Fig. 3. This curve was obtained by numerical iterations and represents the location separating the region of positive largest Lyapunov exponent ($\sigma_1>0$) from that of zero σ_1. The Lyapunov exponents were defined in the usual way and calculated

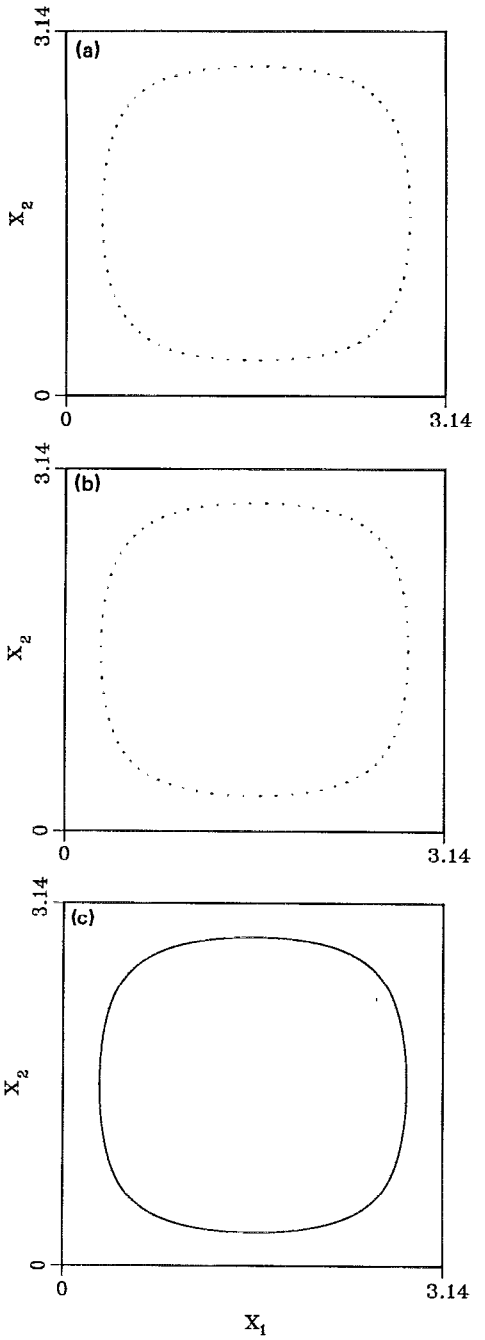

FIG. 2. A typical fluid trajectory and test of integration scheme. (a) Fluid position at the first 100 time units; (b) fluid positions at the last 100 time units (from 9901 to 10 000); (c) fluid positions at all 10 000 time units.

following the procedures of Wolf *et al.*[17] The largest Lyapunov exponent was computed based on a particle trajectory in the time interval between 2000 and 4000, and was considered to be positive if its value was larger than 0.005. The initial particle location was (1.6,1.6). Seven representative points on the boundary were actually iterated to form the smooth curve, although the exact boundary may not be smooth. The boundary curve can be approximated by $\mathrm{St}\cdot R \approx 1$. The fact that the chaos region is above the

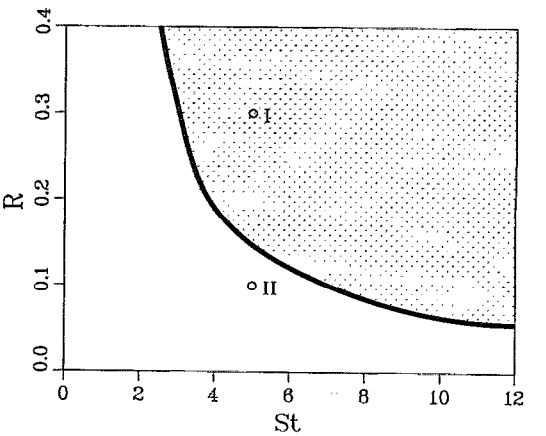

FIG. 3. The regions for chaotic and periodic particle motion in the parameter space. Particle motion is chaotic in the shaded region and periodic in the remaining region. The two points indicate the two representative cases. I: (St=5,R=0.3); II: (St=5,R=0.1).

curve (i.e., $\mathrm{St}\cdot R \geqslant 1$) indicates that the pressure gradient force is significant compared to the drag force in such a region. In the limit for heavy particles, where the particle density is much larger than the fluid density ($\rho_p/\rho_f = \infty$), i.e., R=0.0, the particle motion is always periodic.

To test the effect of initial location on the long-time behavior of the particle orbit, we compute the probability density function (pdf) of the short-time, average exponential growth rate of infinitesimal variations along particle trajectories following Varosi *et al.*[18] In the long term this average will converge to give the largest Lyapunov exponent. Figure 4 shows the pdf function at three different times for the case of St=5.0 and R=0.3. The pdf was found using 40 000 points starting from a uniform grid in the square $0 < (x_1, x_2) < \pi$. Of significance is the fact that the pdf is not bimodal, as would be the case if there was a dependence on initial position. As time increases, the pdf is sharpened with the peak location approaching the value of the largest Lyapunov exponent from below. At t=100,

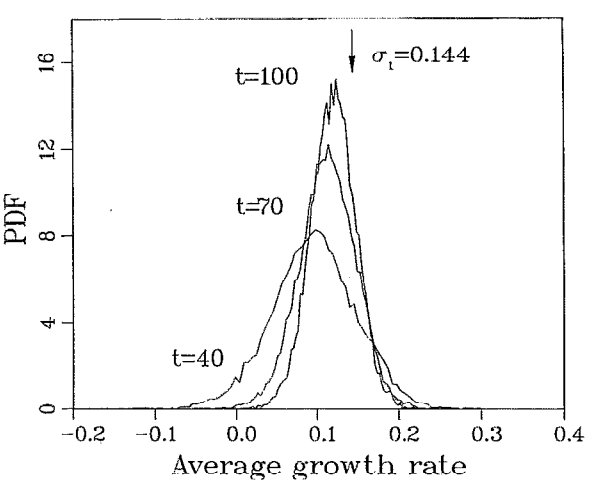

FIG. 4. The pdf function of a short-time Lyapunov exponent for a given set of system parameters.

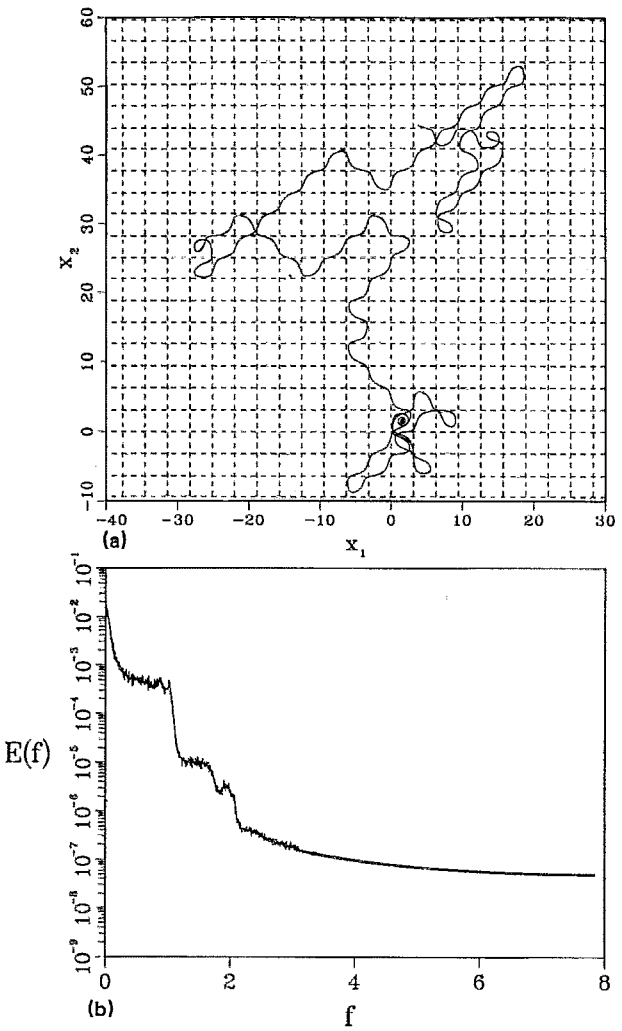

FIG. 5. (a) A typical trajectory of a particle in the chaos region with St=5 and R=0.3. Initial particle location is (1.6,1.6). Dashed lines mark the cell boundaries. (b) The power spectra for the particle velocities in the x_1 and x_2 directions for the same condition.

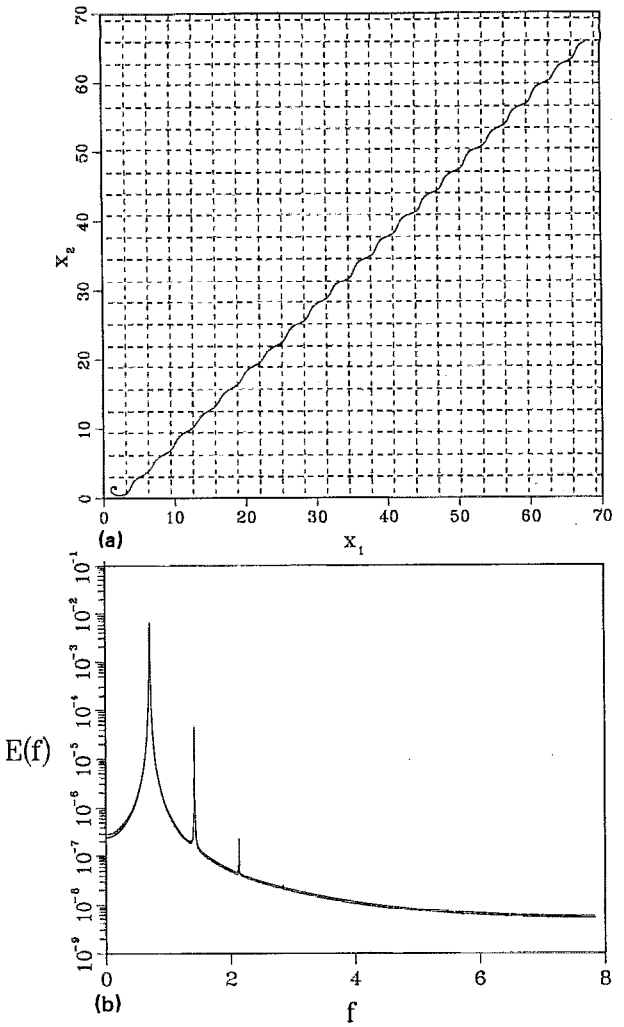

FIG. 6. (a) A typical periodic trajectory of a particle with St=5 and R=0.1. Initial particle location is (1.6,1.6). (b) The power spectra for the particle velocities in the x_1 and x_2 directions for the same condition.

almost all the points have a positive average exponential growth rate. We expect that all the points will have a similar, single asymptotic growth rate when $t \to \infty$, indicating that the long-term behavior is unique and independent of the initial location. Further evidence is presented later when the ergodicity of the system is discussed.

A typical trajectory for the chaotic motion is shown in Fig. 5. The parameters used in this calculation are shown in Fig. 3 as point I. This set of parameters will be referred to as case I in later discussions. The initial particle location (1.6,1.6) is near the center of the cell. The particle moves along an outward spiral curve for some initial time due to inertial (centrifugal) force. The long-time motion is very irregular. The centrifugal effect does not allow the particle to stay in any cell for long. Actually the particle seldom visits the center of the cell where the vorticity is strong. At times the particle cuts through the cell boundary and enters a new cell. This process repeats nonperiodically. Also shown are the power spectra of the particle's velocity at long time. There is no difference between the v_1 spectrum and v_2 spectrum as expected. The broadband frequency contribution indicates the motion is chaotic. The power spectrum was obtained by taking a long time series of particle velocity (with 2048×50 data points) at a sampling rate of 2.5 samples per time unit. The VFFTPK library on Cray-YMP at the Pittsburgh Supercomputing Center (PSC) was used to derive the Fourier coefficients.

Figure 6 shows a typical particle trajectory when the motion is periodic. It will be referred to as case II and the parameters are shown as point II in the parameter space of Fig. 3. In this case the particle travels along a 45° zigzag curve. The power spectrum has a strong peak at the fundamental frequency and its harmonics. The period is about 8.64 time units. In contrast with the periodic motion of fluid elements where the orbit is closed streamlines, the periodic motion of the aerosol particles follows an open trajectory. In other words, the particle inertia destroys closed periodic orbits and in turn can generate open periodic orbits. It is noted that by open periodic orbits we do not distinguish $(y_1+2m\pi, y_2+2n\pi)$ from (y_1, y_2), where m and n are arbitrary integers.

C. Dispersion and anomalous dispersion

The dispersion characteristics of particle clouds are often of interest in engineering applications. An understanding of the dispersion mechanism can lead to better methods of controlling and predicting the dispersion rate. First we shall clarify what we mean by dispersion. A true dispersion process is what one observes when particles are released into a fully developed turbulent flow. This process is usually described by stochastic dynamics like that used in the classical paper by Taylor.[19] Turbulent dispersion has the following characteristics: (1) In a turbulent flow the Lagrangian velocity is correlated with itself only for a limited time, the integral time T_L. This loss of history leads to very irregular particle trajectories. (2) The mean-square displacement of the particles grows linearly with increasing time for $t \gg T_L$. (3) The probability distribution of displacement is asymptotically normal (for example, see Batchelor and Townsend[20]). The linear growth of the mean-square displacement allows one to define a long-time dispersion coefficient as,

$$\epsilon = \lim_{t\to\infty} \frac{1}{2}\frac{d\langle y^2(t)\rangle}{dt} = \int_0^\infty R(\tau)d\tau, \tag{7}$$

where $R(\tau)$ is the Lagrangian velocity correlation,

$$R(\tau) = \langle v(t)v(t+\tau)\rangle. \tag{8}$$

Angle brackets represent ensemble average over particle trajectories. We will show that all these characteristics can be observed for aerosol particles in the cellular flow if the motion is chaotic.

To visualize how a cloud of aerosol particles evolves, we place 10 000 particles uniformly in the region $0 \leqslant x_1 \leqslant 2\pi$, $0 \leqslant x_2 \leqslant 2\pi$ (four cells) at $t=0$ with an initial velocity of zero. Figure 7 shows the locations of these particles at $t=0$, 120, and 240 for case I. The particles appear to disperse in all directions and the region containing the particles expands with time. The initial square cloud shape is gradually lost as time increases. The probability distribution of the displacement in the x_1 direction, $y_1(t)-y_1(t=0)$, is computed for the particle cloud and shown in Fig. 8 for $t=120$ and 240. It clearly approaches a normal distribution at long time except for an abnormal peak at the center. The peak represents the effect of fixed points in the system. Particles located exactly at these points remain there. The main source of the peak is from the particles located at the cell boundaries (about 400 out of 10 000 particles) at $t=0.0$. These particles will stay on the boundaries and eventually be trapped by a fixed point since cell boundaries are stable manifolds. For example, on the boundary of $0 \leqslant x_1 \leqslant 2\pi$ and $x_2=0.0$ there are two such fixed points,

$$x_1 = \pi \pm \cos^{-1}[1/(\mathrm{St}\cdot R)], \quad x_2 = 0. \tag{9}$$

In addition, particles placed very close to these points take a long time to escape. The contribution of the peak to the overall distribution is small (about 6% at $t=120$ and 5% at $t=240$) and is negligible. The peak can also be eliminated by offsetting the particle initial locations slightly.

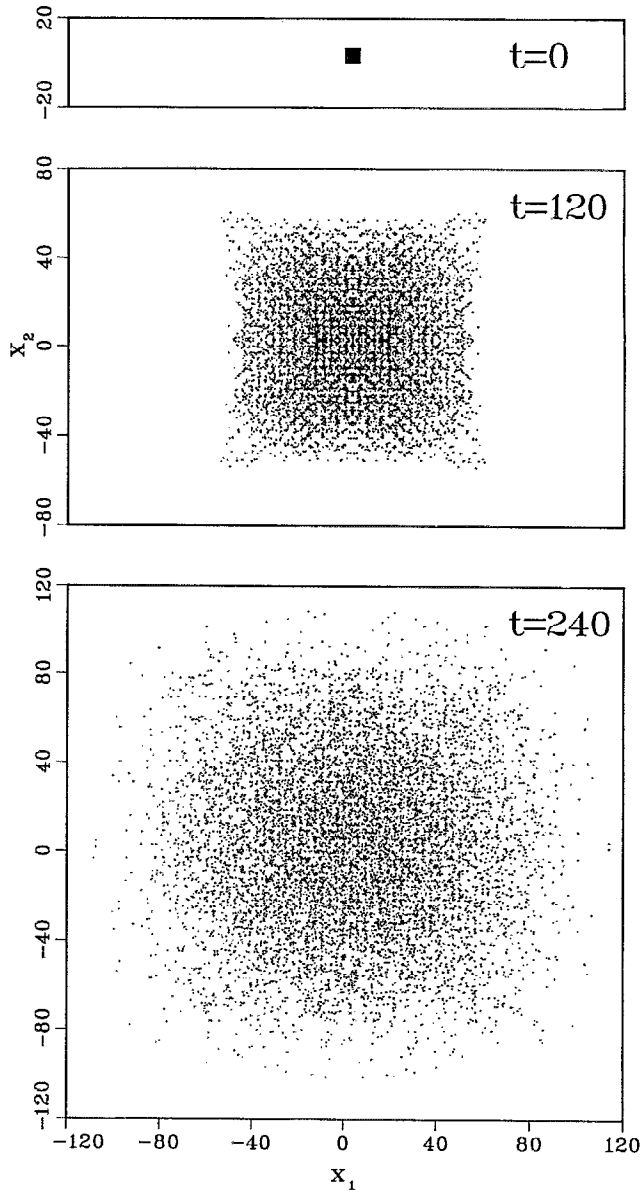

FIG. 7. Position plots at $t=240$ of 10 000 particles that were uniformly distributed in the fundamental box at $t=0$ for case I.

Since the cellular flow field is symmetric the coordinates x_1 and x_2 are interchangeable and the probability distribution is the same in the x_2 direction.

To measure the growth of the particle cloud, we further computed the mean-square displacement (MSD) as a function of time (Fig. 9). Except for some initial transition time, MSD is isotropic and a linear function of time. The slope can be accurately determined from the curve. Based on Eq. (7), the effective diffusivity is computed to be 3.15.

The shape of the velocity correlation can be used to help understand the dispersion dynamics. The velocity correlation was computed from a *single* particle trajectory starting from (1.6,1.6). After the initial transition, a long particle velocity record was taken at a sample rate of 2.5 samples per unit. A total of 2048×50 data points were

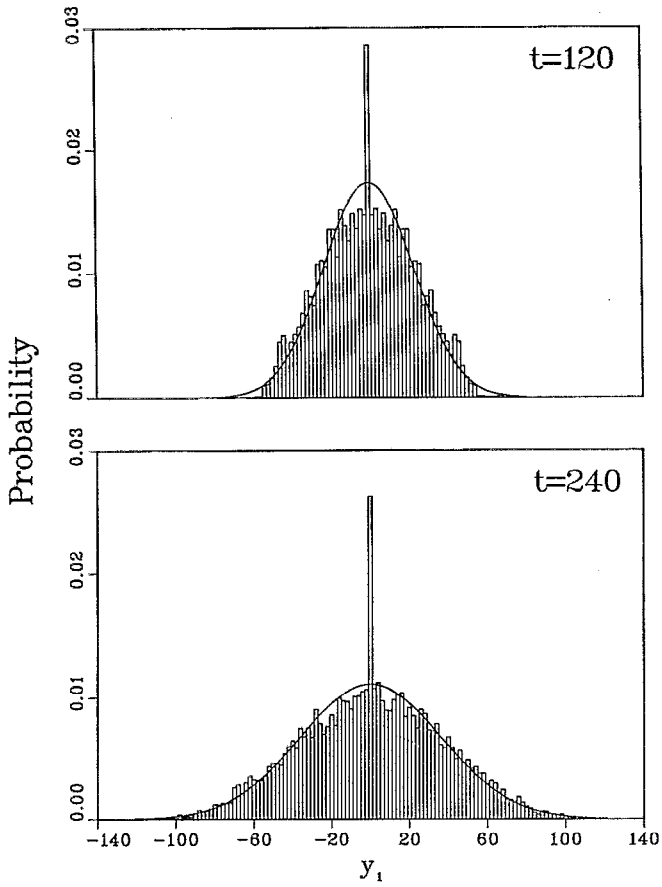

FIG. 8. The probability distribution of particle displacement in the x_1 direction for Fig. 7. The curves are a normal distribution of same standard deviations.

used. The average was taken over time instead of over trajectories since it was assumed, *a priori,* that the Lagrangian motion is statistically stationary and ergodic. Figure 10 gives the results for both v_1 and v_2 velocity components. The velocity correlation decays quickly with time

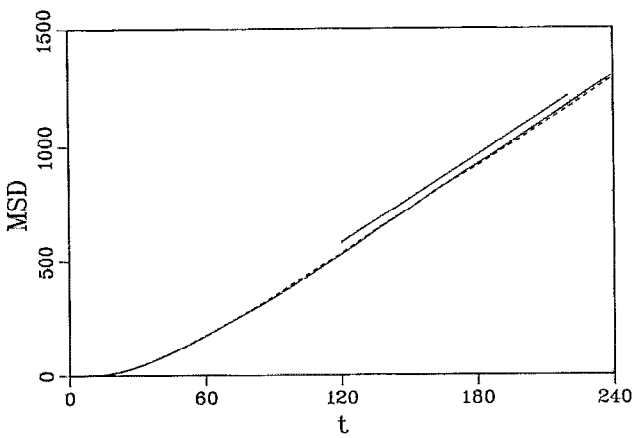

FIG. 9. Mean-square displacement (MSD) for case I as a function of time. MSD was computed based on 10 000 particles that were uniformly distributed in the fundamental box at $t=0$.

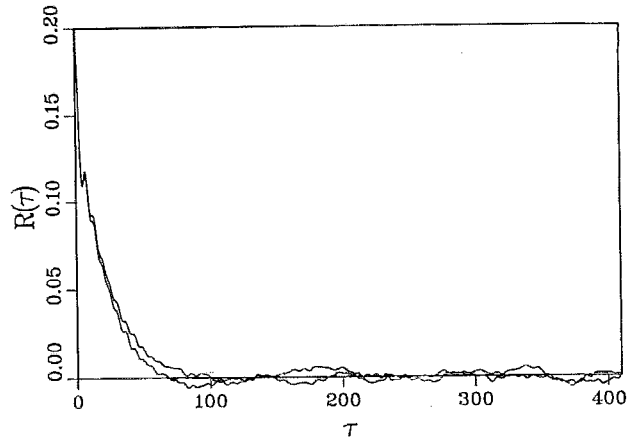

FIG. 10. The Lagrangian velocity correlations for case I.

delay and is approximately zero for long time. This is very similar to Lagrangian velocity correlation in a turbulent flow. The correlation value at zero time delay is 0.1947, which corresponds to a particle root-mean-square (rms) fluctuating velocity of 0.4412. From the correlation curves, the integral correlation time can be estimated to be 16.04 time units. The area under the correlation curve is the effective diffusivity [see Eq. (7)], that is, $\epsilon=0.1947\times 16.04 =3.12$. This value is very close to the value calculated from the MSD. This finding allows us to assume that Taylor's theory of turbulent diffusion is applicable to the Lagrangian motion of aerosol particles in our simple cellular flow. In addition, it confirms, *a posteriori,* that the chaotic motion is ergodic. Further support and discussions for the ergodicity will be given in Sec. II E. The consistency in the diffusivity result also confirms our belief that the initial conditions do not affect the long-time average quantities, since the velocity correlation based on a *single* trajectory gives us the same information as the MSD based on 10 000 particle trajectories. The loss of correlation in the particle velocity due to Lagrangian chaos is the reason for the linear growth of MSD at long time.

To be complete, we will briefly discuss the particle cloud evolution for case II. Again 10 000 particles are placed uniformly in a small region as we did for case I. The particle locations at $t=120$ and 240 are shown in Fig. 11. In this case, the initial cloud splits into four patches and each of the patches moves with a constant velocity along 45° lines in the four quadrants (on a scale much larger than the cell size). The MSD is linearly related to t^2 rather than t since

$$y_i(t)-y_i(0)\rightarrow(\pi/T)t, \tag{10}$$

where T is the period for a particle to travel through a cell of size π. This is verified in Fig. 12 where MSD is plotted as a function of t^2. The slope of the straight line is 0.132 which is exactly equal to π^2/T^2 as expected. This t^2 anomalous dispersion was also observed by Crisanti *et al.*,[5] however, the reason for this behavior is made clearer here.

In summary, our model problem indicates that even for a very simple flow a dispersion process with essentially

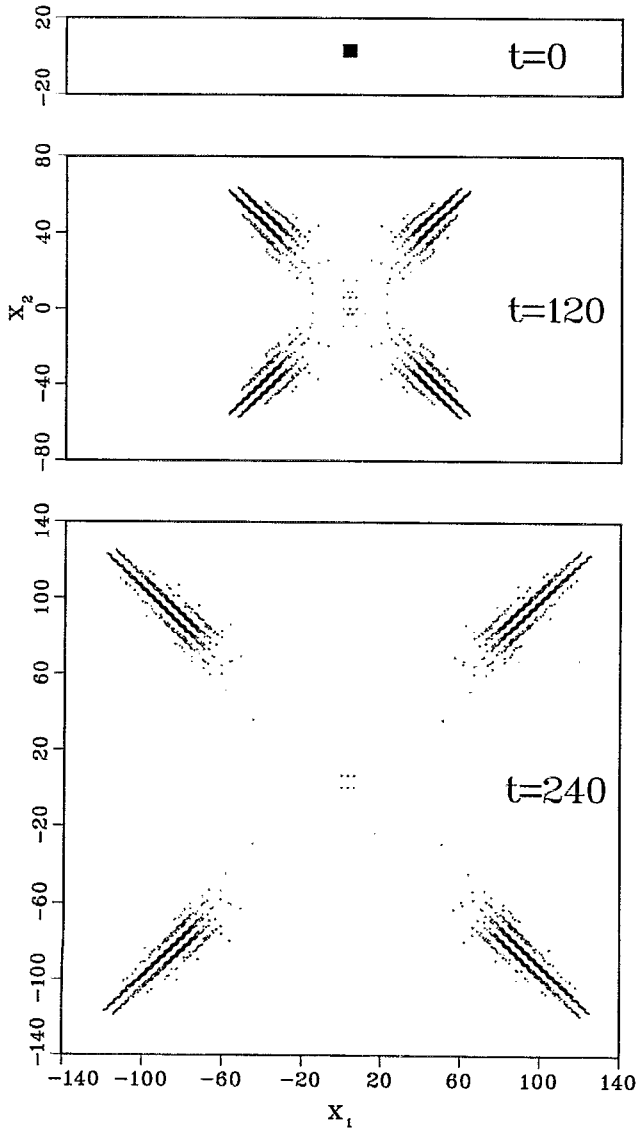

FIG. 11. Position plots at $t=240$ of 10 000 particles were uniformly distributed in the fundamental box at $t=0$ for case II.

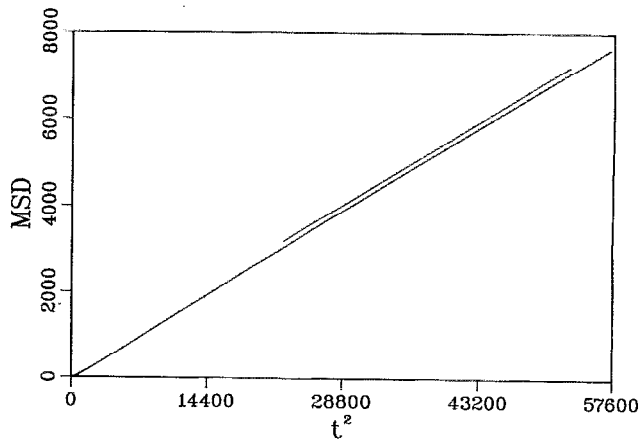

FIG. 12. Mean-square displacement (MSD) for case II as a function of t^2. MSD was computed based on 10 000 particles which were uniformly distributed in the fundamental box at $t=0$.

the same features as turbulent dispersion exists when chaotic Lagrangian motion occurs.

D. Correlation between chaos and dispersion

The system discussed above is fully deterministic and the appearance of Lagrangian chaos is a necessary condition for dispersion. A natural question that arises here is how the degree of chaos and rate of dispersion are correlated. In terms of dynamical systems, the long-time solution of a dissipative nonlinear system is an attractor and the dimension of the attractor is perhaps its most basic property. If the solution is chaotic, the attractor is often called a strange attractor and it has a noninteger dimensionality. Our focus here is to examine how the degree of chaos affects the effective dispersion rate and what measure of an attractor best correlates with the diffusivity. Farmer *et al.*[21] reviewed a number of different definitions of attractor dimension. Of the definitions they discussed, the Lyapunov dimension, which is defined in terms of Lyapunov exponents, is usually much easier to calculate than any other. Lyapunov exponents characterize the mean exponential rate of divergence of neighboring trajectories from a given reference trajectory in phase space. A positive maximum Lyapunov exponent indicates that the individual solution (but not average feature or measure) of the system is very sensitive to its initial conditions. Therefore, we explored the quantitative correlation of diffusivity with Lyapunov dimension and tried to provide a physical basis for such a correlation.

For our autonomous four-dimensional system given by (5a)–(5d), there exist four Lyapunov exponents. They can all be computed by the standard procedure as given by Wolf *et al.*[17] We used the same method in our earlier papers[8,9] and we assumed the values of Lyapunov exponents for our system were independent of the initial particle location due to the property of ergodicity (except for isolated fixed points). The Kaplan–Yorke conjecture[22] was

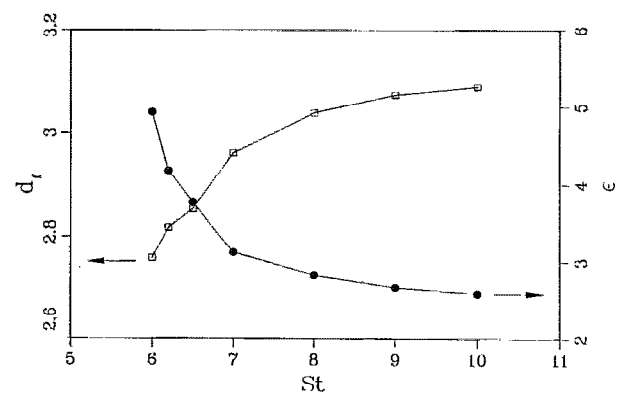

FIG. 13. Fractal dimension and effective diffusivity as a function of St for $R=0.2$.

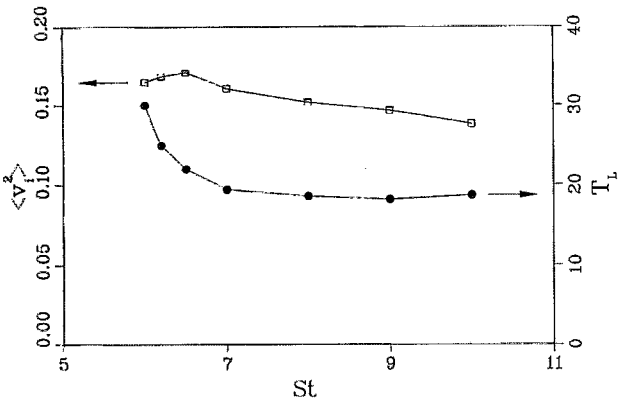

FIG. 14. Particle mean-square fluctuating velocity and integral correlation time as a function of St for $R=0.2$.

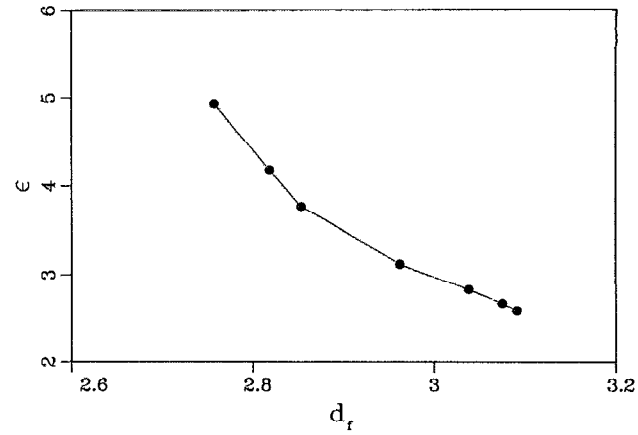

FIG. 15. Diffusivity as a function of fractal dimension for $R=0.2$ and varying St.

then used to derive a fractal dimension based on the Lyapunov exponents.

We restrict our discussion to a fixed density ratio, $R=0.2$, and vary St over the region of chaos of the parameter space (Fig. 3). Both fractal dimension and diffusivity are plotted as a function of St in Fig. 13. For the parameter range shown in Fig. 13, we note that only the largest Lyapunov exponent is positive, the next one is zero, and the other two are negative. As St increases, the drag force becomes less and less important as compared to the pressure gradient force. The pressure gradient force causes a particle to become temporarily trapped in a cell, thus for larger St a particle tends to stay longer in a cell before entering a new cell. This means that a particle orbit may visit more space in each cell (cf. next section). In addition, the cell size represents the smallest scale of the particle orbit and the fractal dimension is a measure of fine-scale structure of the orbit. Therefore, the attractor is likely to take on a larger dimension as St increases. On the other hand, the dispersion rate is reduced for two reasons. First the rms fluctuating velocity decreases as St increases and, second, frequent trapping of the particle by cells also results in a loss of large-scale particle velocity correlation. In fact, the second reason dominates the reduction of dispersion rate, as is shown by Fig. 14. The mean-square particle fluctuating velocity seems to decrease with increasing St. But near St=6.0, it actually increases slightly with St. The velocity correlation time drops very quickly for relatively small St but then appears to change slowly for relatively large St. Since the nature of the particle motion is mainly determined by the product $\mathrm{St}\cdot R$, increasing R for a fixed St should give similar results as increasing St for a fixed R.

The diffusivity is plotted as a function of fractal dimension in Fig. 15, and a definite correlation is observed. The diffusivity decreases monotonically with increasing fractal dimension. Figure 16 shows diffusivity as a function of the positive Lyapunov exponent. The correlation is less clear than that between diffusivity and fractal dimension.

E. Nonuniform distribution and mixing in physical space

The dispersion discussed above represents the particle motion on a large scale compared to the cell size. In this subsection we examine particle distribution on a scale comparable to the cell size, small-scale mixing.

Suppose that a large number of particles are uniformly distributed in the space (not just a single cell) at $t=0$. We are interested in the asymptotic distribution of the particles after a long time. Because of the spatial periodicity of the Eulerian flow field, the procedure that can be used to find this distribution is[13] (1) uniformly place a large number (say 10 000) of particles in the fundamental box containing four cells, $0\leqslant x_1\leqslant 2\pi$ and $0\leqslant x_2\leqslant 2\pi$; (2) solve for the long-time location of all particles numerically, where long time means much longer than the correlation time for chaotic trajectories; and (3) instead of plotting the true locations as we did in Fig. 7, truncate the position coordinates of particles to the fundamental box by taking the modulo with respect to 2π. Other reflectional symmetries in the

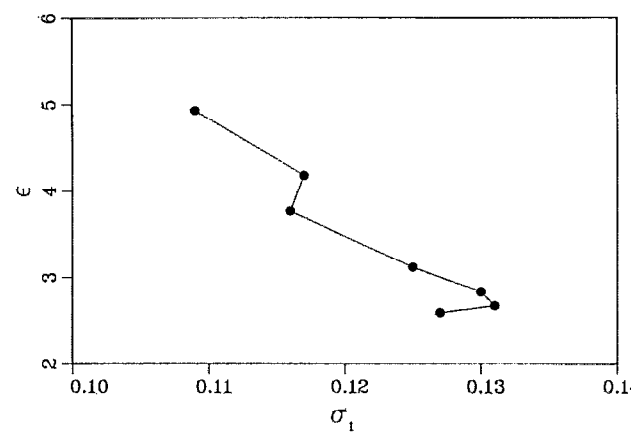

FIG. 16. Diffusivity as a function of the largest Lyapunov exponent for $R=0.2$ and varying St.

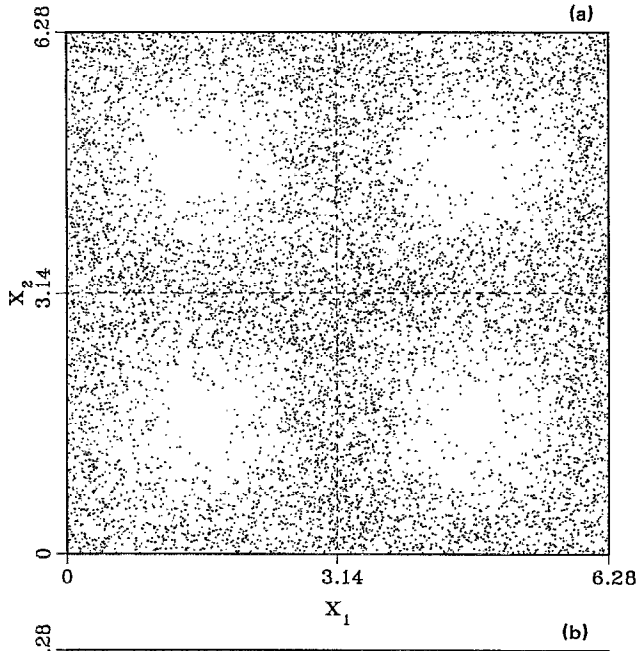

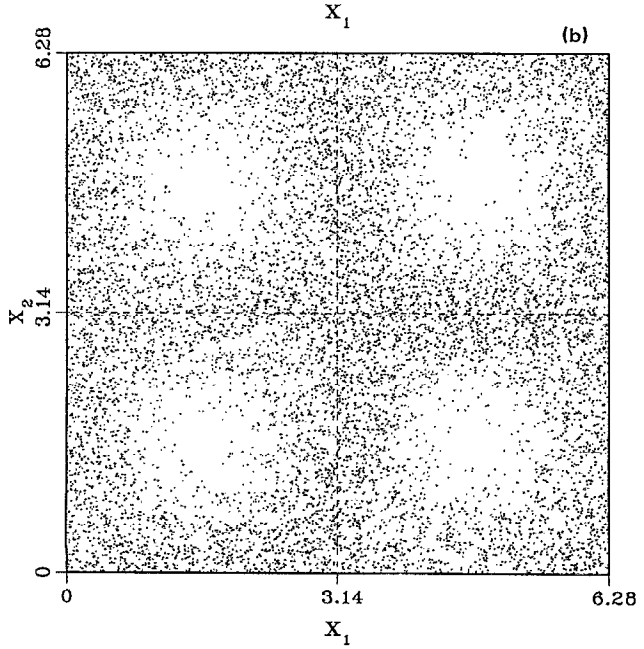

FIG. 17. (a) Position plots for 10 000 particles at time $t=240$ for case I. The particles are placed uniformly in the fundamental box at $t=0$. (b) Position plots for a single particle at 10 000 time steps starting from $t=200$ with step size equal to one. Initial particle location is (1.6,1.6).

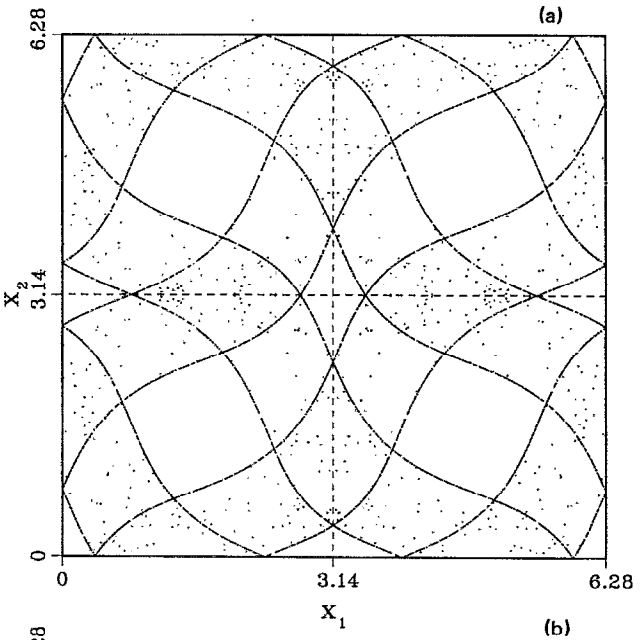

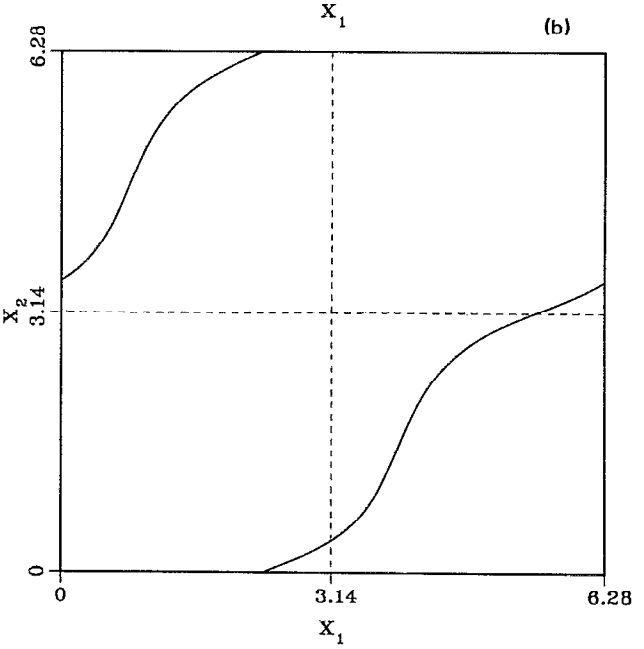

FIG. 18. (a) Position plots for 10 000 particles at time $t=240$ for case II. The particles are placed uniformly in the fundamental box at $t=0$. (b) Position plots for a single particle at 10 000 time steps starting from $t=200$ with step size equal to one. Initial particle location is (1.6,1.6).

fundamental box can be used to reduce the actual number of initial particles considered.

Figure 17(a) shows the position of 10 000 particles at $t=240$ for case I. The asymptotic concentration is not uniform. In a small region near the center of each cell, the local particle concentration is about zero. The maximum concentration appears to occur at the saddle points or corners of each cell.

To help understand if the system is ergodic and to study the mixing property, we consider the asymptotic probability of a single particle visiting a given region in space. Figure 17(b) shows locations visited by a single particle starting from $t=200$ with a uniform step size of one and continuing for 10 000 time steps. The initial particle location is again (1.6,1.6). The single particle more frequently visited the region near the cell boundaries and we find that Fig. 17(b) is almost identical to Fig. 17(a). The equivalence of position probability for a single particle and the concentration distribution for a cloud of particles indicates ergodicity of the dynamical system (see Aref[23]). Ergodicity and exponential stretching of material lines (a characteristic of chaotic systems) implies efficient mixing of particles. We notice that for fluid elements a single element only visits a closed streamline, therefore, the position

probability of a single particle is very different from the concentration distribution of particle cloud. This indicates poor mixing of fluid elements, with no mixing among different streamlines.

The position plots for case II are given in Figs. 18(a) and 18(b). Figure 18(a) shows the particle cloud starting to accumulate into isolated curves. This type of movement has been discussed by Maxey and Corrsin.[13] At $t=240$, there is still a small portion of particles in the clouds located away from the accumulation curves. Figure 18(b) shows the positions at 10 000 time steps of a single particle. All the points fall on two well-defined line segments which are the image of a periodic orbit in the box. The region taken up by the curves in Fig. 18(b) is one-eighth of the region taken up by the curves in Fig. 18(a). The mixing in case II is poor as compared to case I for two reasons; first, a single particle only visits a portion of the attraction curves, and second, the attractor region forms isolated curves instead of nearly space-filling, spreading sets.

Finally, we compared the position plots for St=6.0 and 10.0 given $R=0.2$. For both cases the Lagrangian motion is chaotic and the position probability of a single particle was found to be the same as the concentration distribution of particle cloud. Thus we only provide the position plots of particle clouds at $t=240$ in Fig. 19. Further reflectional symmetry, i.e., $\pi+y_1\to\pi-y_1$ and $\pi+y_2\to\pi-y_2$, was used to reduce the region of $0\leqslant y_1,\ y_2\leqslant 2\pi$ to a single cell $0\leqslant y_1,\ y_2\leqslant\pi$ for the position plots. The concentration distribution for St=10.0 is more uniform than for St=6.0. Actually there is a void in the center of the plot for St=6.0. (Note that a particle starting within the void region will eventually move away from the region, i.e., the void is a result of the asymptotic evolution of the system and not a reflection of the system dependence on the initial location.) While for St=10 the concentration distribution is almost uniform. This is very interesting because the case of St=10 and $R=0.2$ approaches the definition of *dynamical system (DS) mixing* (Aref[23]). Dynamical system mixing is a desirable property since it indicates efficient mixing. It is surprising that it can be asymptotically achieved for aerosol particles in a regular flow field! In fact, for all the parameter combinations in the region where chaos is found (see Fig. 3), the Lagrangian motion has the property of ergodicity. For our model problem in the chaos region, the more uniform the concentration distribution, the closer the system approaches DS mixing, i.e., the better the mixing efficiency. To further quantify the degree of nonuniformity in the concentration distribution, we computed the relative concentration variance using

$$\frac{\overline{\left(c(x_1,x_2)-\overline{c(x_1,x_2)}\right)^2}}{\overline{\left(c(x_1,x_2)\right)^2}} \equiv \frac{\langle \delta c^2\rangle}{\bar{c}^2}=\pi^2\int_{0\leqslant x_1,x_2\leqslant\pi}\left(c(x_1,x_2)-\frac{1}{\pi^2}\right)^2 dx_1\,dx_2. \quad (11)$$

The overbars denote the average over space. The region, $0\leqslant x_1,\ x_2\leqslant\pi$, was discretized by a uniform grid of $m\times m$,

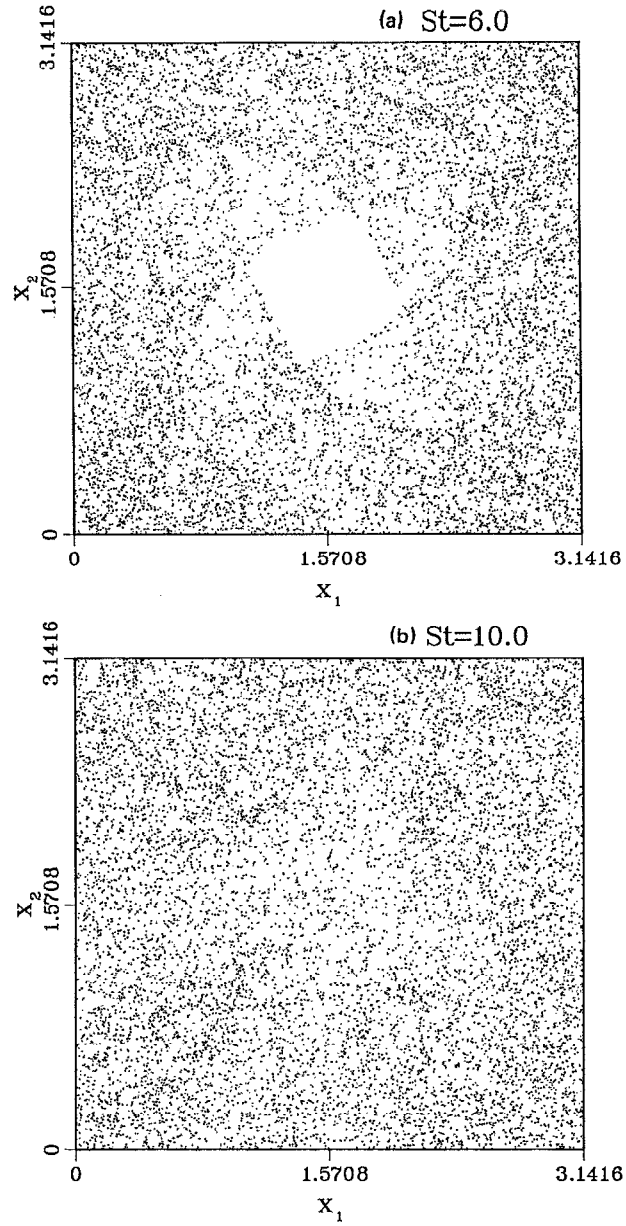

FIG. 19. (a) Position plots for 10 000 particles at time $t=240$ for St=6.0 and $R=0.2$. The particles are placed uniformly in the fundamental box at $t=0$. Reflectional symmetry was used to replace all the particles in a single cell. (b) Same as (a) for St=10.0 and $R=0.2$.

and the number of particles in each grid cell, n_i, was counted. If N is the total particle number, then

$$\frac{\overline{\left(c(x_1,x_2)-\overline{c(x_1,x_2)}\right)^2}}{\overline{\left(c(x_1,x_2)\right)^2}}=\sum_i \frac{1}{m^2}\left(\frac{n_i m^2}{N}-1\right)^2, \quad (12)$$

$N=10\,000$, and $m=50$ were used. The portion of particles attracted by fixed points was not counted. Figure 20 shows the relative concentration variance as a function of St. The concentration tends toward a uniform distribution as St increases. In Sec. II D, we found that the diffusivity decreases and the fractal dimension increases as the St increases. These results indicate that the larger the fractal dimension the better the particles will be mixed.

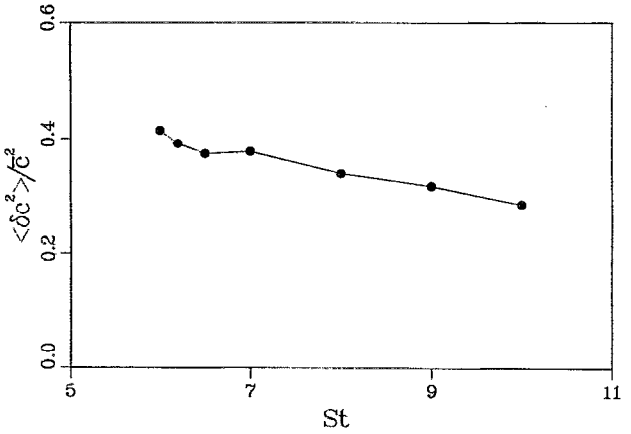

FIG. 20. Relative concentration variance as a function of St for $R=0.2$.

III. HEAVY PARTICLES IN A SHEAR MIXING LAYER

In the discussion of Lagrangian motion of aerosol particles in a cellular flow, it was shown that a large dispersion rate correlates with small fractal dimension. It is also shown that an increase in the fractal dimension leads to better mixing efficiency, i.e., toward DS mixing. Therefore, large dispersion corresponds to a low degree of chaos and relatively low mixing efficiency. We would expect to find similar correlations between dispersion and mixing (or degree of chaos) in more realistic flows such as a plane mixing layer that have features in common with cellular flows. We provide here some preliminary and qualitative results for the motion of heavy particles in such flow. A detailed study of this subject is beyond the scope of the present paper.

We consider a two-dimensional, incompressible, viscous, and temporally evolving mixing layer. The flow originates from a prescribed initial mean velocity profile and nonlinear instability of certain perturbations. The main activity of the mixing layer flow is the development of a localized roll of vortices and their subsequent pairing. Such a plane mixing layer and the cellular flow have many similar characteristics as well as many differences. The most striking similarity is the significant role played by the rotational motion of the fluid, i.e., vortical structures. The passive motion of particles denser than the fluid is then controlled by the inertial centrifugal effect. Some differences are also noted as a reminder that only qualitative comparisons should be made for Lagrangian particle motion between the two flows. The mixing layer flow is unsteady and not periodic in the vertical direction. In addition the vertical dispersion for a mixing layer is measured on the scale of vortices, in contrast with the cellular flow where the dispersion is usually measured on a scale much larger than the cell size. The mixing property will also be defined differently.

The dispersion of heavy particles in a mixing layer has been an active research area in recent years. For example, the interaction between the particles and the large-scale vortical structures has been addressed by Crowe *et al.*[24] and studied experimentally by Lazaro and Lasheras.[25] Chung and Troutt[26] and Chein and Chung[27] calculated the particle dispersion rate using discrete point vortices to simulate the flow. The main finding of these studies was that particles of intermediate inertia can disperse at rates greater than for fluid elements. The larger dispersion is due to the vortical structure of the flow, which produces a centrifugal effect which in turn drives the particles toward the edge of the vortical region. However, the mixing property of particles has been overlooked in these earlier studies.

Consider a mixing layer governed by the two-dimensional incompressible Navier–Stokes equations (in dimensionless form):

$$\frac{\partial u}{\partial x}+\frac{\partial w}{\partial z}=0, \tag{13a}$$

$$\frac{\partial u}{\partial t}+u\frac{\partial u}{\partial x}+w\frac{\partial u}{\partial z}+\frac{\partial P}{\partial x}=\frac{1}{\mathrm{Re}}\left(\frac{\partial^2 u}{\partial x^2}+\frac{\partial^2 u}{\partial z^2}\right), \tag{13b}$$

$$\frac{\partial w}{\partial t}+u\frac{\partial w}{\partial x}+w\frac{\partial w}{\partial z}+\frac{\partial P}{\partial z}=\frac{1}{\mathrm{Re}}\left(\frac{\partial^2 w}{\partial x^2}+\frac{\partial^2 w}{\partial z^2}\right). \tag{13c}$$

Here x and z are coordinates in the horizontal direction and the vertical direction, u and w are fluid velocity components, and P is static pressure. The Reynolds number, Re, is based on the free-stream velocity and initial vorticity layer thickness. The initial velocity field is

$$u(x,z,t=0)=\tanh(z), \quad w(x,z,t=0)=0. \tag{14}$$

It is well known that such an initial layer is unstable under small perturbation due to Kelvin–Helmholtz instability. The flow was solved by direct numerical simulation on a grid resolution of 128×128. Full Fourier expansion was applied to flow velocity and vorticity in the x direction and sine/cosine expansion was used in the z direction. The original code was developed to study the structures of stratified shear layers and a detailed description can be found in Wang *et al.*[28] The eigenfunctions of linear instability were used for initial perturbation. Both fundamental and subharmonic waves with wave number $\alpha_1=0.4446$ and $\alpha_2=0.2223$ were used in the initial perturbation to simulate vortex roll-up and pairing. The perturbation amplitude for both waves was 0.05. Periodic boundary conditions were used in the x direction. The simulation box had a size of $2\pi/\alpha_2$ (or 28.26) in the x direction and 24.00 in the z direction.

To illustrate the difference between dispersion and mixing of particles, we placed two lines of particles horizontally above and below the center of the layer at $z=\pm1$. Each line was formed by 1000 uniformly distributed particles. The motion of each particle was found numerically. Hermite interpolation[29] was used to obtain the fluid velocity at the particle's location and the initial velocity of the particle was set equal to the local fluid velocity. Two kinds of particles, i.e., fluid elements and heavy particles, were studied. Fluid elements were convected by the local fluid velocity. Equation (2) with $R=0$ was used to calculate the motion of the heavy particle, which means only a Stokes

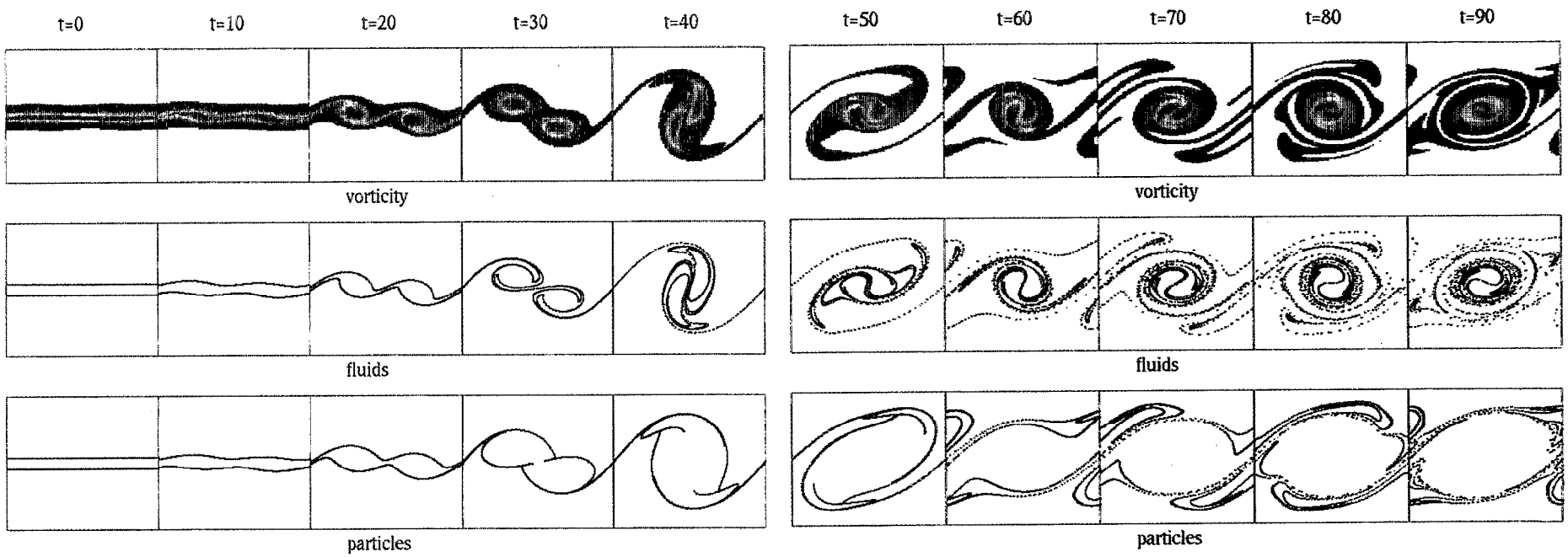

FIG. 21. Evolution of vorticity distribution for the shear layer and material lines for fluids and heavy particles.

drag force and particle inertia were considered. The inertia parameter St was set to one. In the numerical simulations, only one material line at $z=1.0$ was computed since the material line at $z=-1.0$ can be derived from the symmetry consideration, i.e., a mapping $(x,z)\rightarrow(h_x-x,-z)$ where h_x is the box size in the x direction.

Figure 21 shows the numerical results for Re=300. The vorticity distribution, fluid particle positions, and heavy particle positions are plotted from $t=0.0$ to 90 for every ten time units. The roll-up of the fundamental wave occurs at $t=20$ and the pairing of the fundamental vortices takes place immediately as a result of nonlinear growth of the subharmonic component. The merging of vortices gives rise to a larger vortical region as well as increased viscous diffusion. The development of the shear layer instability is well known and is in agreement with other studies (e.g., Corcos and Sherman[30]). The main focus of the simulation is to study how the particles are dispersed and mixed. The fluid material lines are stretched by the straining field at the braids and at the center before pairing, and folded by the rotational motion inside the vortical regions. Most of the fluid particles are captured by the vortical region as the region grows. During this process the two material lines are brought very close together and mixed. The stretching and folding does not happen as rapidly for the heavy particles due to inertia effects. Heavy particles do not enter the vortical regions due to the centrifugal effect, which leads to a void region in the center of the box. This void region grows as time increases. The material lines of heavy particles have a relatively simple geometry which resembles the edge of the vortical structure. This process leads to a larger vertical dispersion of the heavy particles. Also, we notice that the two material lines of heavy particles are not mixed efficiently since some portions of the lines stay in distinct regions of the box. However, there are certain regions, for example, near the inner edge of the void region, where the mixing of heavy particles is efficient *locally*.

We now proceed to make a quantitative comparison of the dispersion rate and mixing rate between the fluid particles and the heavy particles. The vertical dispersion can be quantified by the mean-square displacement, which is defined in the usual way as

$$\mathrm{MSD}=\frac{1}{N}\sum_{i=1}^{N}[z_i(t)-z_i(t=0)]^2, \tag{15}$$

where N is the number of particles and $z_i(t)$ is the vertical position of the ith particle at time t. The term *mixing* is used here to describe the rate at which the two spatially separated (unmixed) particle sources introduced initially approach each other and become homogenized. The two line sources may be viewed as two point sources for a spatially evolving mixing layer. Similar configurations have been used to study the mixing of a continuous, passive scalar field and interaction between the sources in turbulent flows.[31] The mixing of scalars by homogeneous turbulent flows is usually quantified in terms of the intensity of scalar fluctuations.[32,33] Small scalar fluctuations imply a high degree of homogenization and good mixing. The use of concentration fluctuations is not feasible for our problem since the flow is highly inhomogeneous and the concentration of particles is not continuous for the limited number of particles considered. (Even with a large number of particles the concentration will depend on the length scale over which it is defined.) Instead, we introduce a measure called mixing percentage, which should measure the degree of homogenization on the average, to quantify the mixing process of the two material lines. Mixing percentage is defined as the ratio of the number of particles mixed to the total number of particles. A particle "A" is viewed as being mixed if at a given instant of time at least one other particle "B" from the second material line can be found in some small circular region near the particle "A,"

$$[x_A(t)-x_B(t)]^2+[z_A(t)-z_B(t)]^2<r^2;\qquad z_A(t=0)\neq z_B(t=0). \tag{16}$$

The mixing percentage depends on the value used for r. We used $r=0.4$ which is one-fifth of the initial spacing between the two material lines. This value is chosen to ensure that no particle is mixed initially, but most fluid particles are indeed mixed at the end of the simulation. Figure 22(a) shows the vertical MSD for the fluid particles and the heavy particles. The MSD for the fluid particles is slightly larger than for heavy particles for $t<40$ and has a maximum of 0.042 at $t=40$. It appears to saturate at longer times. The MSD for the heavy particles, however, increases monotonically and becomes much larger than for the fluid

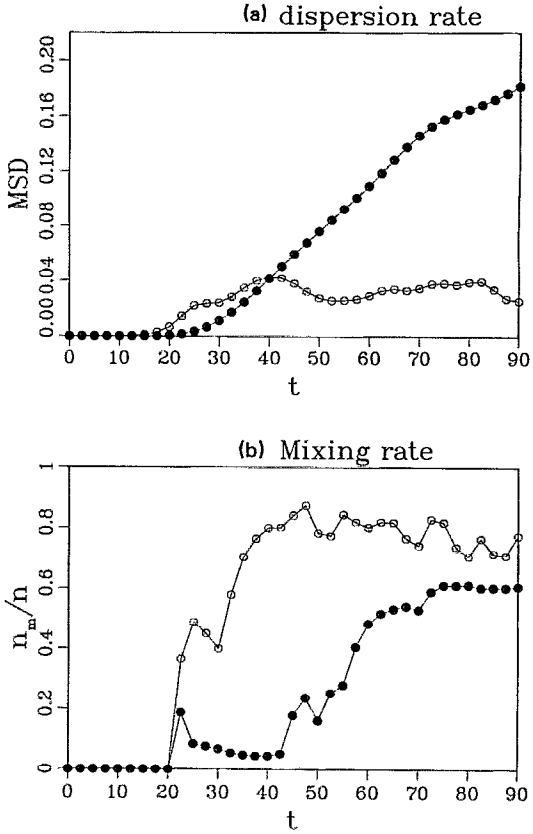

FIG. 22. Comparison of dispersion and mixing between fluids and heavy particles in the shear layer.

particles at large time due to the accumulation of heavy particles at the edge of the vortical region. The mixing percentage as a function of time is shown in Fig. 22(b). The mixing percentage for fluid elements is much larger than for heavy particles at all times. The maximum is 87% at $t=47.5$ for the fluid particles, and 61% at $t=80$ for the heavy particles. The fact that the mixing for fluid elements is better than for heavy particles can also be realized as the following. Imagine that both the fluid particles and heavy particles are introduced in the computation box with a same uniform concentration. The concentration for fluid particles remains uniform for a long time since the flow is incompressible. However, the concentration for heavy particles will not be uniform since no heavy particles stay in the center region for a long time. In other words, if the fluid particles are well mixed with the fluid initially they remain well mixed at all times. This is not true for heavy particles. In summary, the comparison indicates that larger dispersion correlates with a smaller degree of mixing in a shear mixing layer.

IV. CONCLUDING REMARKS

The motion of aerosol particles in a regular, steady, and two-dimensional cellular flow was analyzed numerically and found to be very different from the motion of nondiffusive fluid elements. Aerosol particles move along open orbits which cross over the cell boundaries. These orbits can be either chaotic or periodic depending on the system parameters, i.e., Stokes number and density ratio. (Under certain conditions, closed periodic orbits or other regular asymptotic solutions may exist.) In general, the dispersion of aerosol particles which have chaotic orbits shares many features of Lagrangian dynamics in turbulent flows. It can enhance the mixing process of particles since the chaotic advection has the property of ergodicity. However, one should distinguish dispersion from mixing for this two-dimensional, well-organized circulation flow. In fact it was shown that high dispersion rate is correlated with low fractal dimension and low mixing efficiency. A similar correlation between dispersion and mixing was found for particles convected by a plane shear mixing layer.

It is worth noting that the dispersion of aerosol particles in the cellular flow is somewhat similar to the Taylor longitudinal dispersion.[34] Both dispersions are strongly affected by flow advection. The longitudinal dispersion coefficient in a pipe is inversely proportional to the transverse diffusivity or the radial mixing rate. The time scale that is needed for the dispersion in our system to become a valid description, i.e., the integral time of the velocity correlation, is usually much greater than both the particle response time and the time scale of the flow. This is also a feature of the Taylor longitudinal dispersion, i.e., the time scale for the longitudinal dispersion to become established is much larger than for the transverse dispersion.

In this study, only the long-time characteristics of mixing and dispersion for chaotic particle motion are considered. The dispersion coefficient is a useful description for our system because the chaotic orbits are not bounded and the long-time motion is ergodic or spatially homogeneous. It is also equivalent to long-time two-particle, relative dispersion. For many other well-known systems, such as the blinking-vortex system[1] or the journal-bearing flow,[3] the chaotic motion is confined to a region of finite size, then a dispersion coefficient cannot be easily defined. The analysis of short-time dispersion and mixing for our system is a more difficult problem and remains to be resolved.

Another interesting feature of the Lagrangian turbulence in our *dissipative* system is that the chaotic behavior is independent of the initial particle location and the region of chaos in physical space may appear to be space filling, provided the system evolves for a long enough period. Only the isolated equilibrium points and cell boundaries are different. In many *nondissipative* systems exhibiting Lagrangian turbulence,[1-3] the regions of chaos are localized in space or separated by regions of regular motion.

The results presented here are limited to aerosol particles of zero settling velocity. The gravitational settling has the effect of modifying the flow field and in turn the correlation between dispersion and chaotic mixing may be altered. The effect of settling on the chaotic motion and dispersion rate is currently under investigation and will be reported in a separate paper. The parameter range for Stokes number St is also limited since it is costly to simulate the motion of particles at very large St. The question of whether the particle motion for very large St is chaotic remains open.

ACKNOWLEDGMENTS

LPW is grateful to Dr. D. B. Goldstein for his helpful conversations and suggestions.

This research was supported by a DARPA–URI award and with additional support from the Office of Naval Research. Part of the simulations was done at the Pittsburgh Supercomputer Center.

[1] H. Aref, "Stirring by chaotic advection," J. Fluid Mech. **143**, 1 (1984).
[2] T. Dombre, U. Frisch, J. M. Greene, M. Hénon, A. Mehr, and A. M. Soward, "Chaotic streamlines in the ABC flows," J. Fluid Mech. **167**, 353 (1986).
[3] J. M. Ottino, *The Kinematics of Mixing: Stretching, Chaos, and Transport* (Cambridge U.P., Cambridge, 1989).
[4] M. R. Maxey, "On the advection of spherical and non-spherical particles in a non-uniform flow," Philos. Trans. R. Soc. London Ser. A **333**, 289 (1990).
[5] A. Crisanti, M. Falcioni, A. Provenzale, and A. Vulpiani, "Passive advection of particles denser than the surrounding fluid," Phys. Lett. A **150**, 79 (1990).
[6] R. Mallier and M. Maxey, "The settling of nonspherical particles in a cellular flow field," Phys. Fluids A **3**, 1481 (1991).
[7] J. B. McLaughlin, "Particle size effects on Lagrangian turbulence," Phys. Fluids **31**, 2544 (1988).
[8] L. P. Wang, T. D. Burton, and D. E. Stock, "Quantification of chaotic dynamics for heavy particle dispersion in ABC flow," Phys. Fluids A **3**, 1073 (1991).
[9] L. P. Wang, T. D. Burton, and D. E. Stock, "Chaotic dynamics of heavy particle dispersion: Fractal dimension versus dispersion coefficients," Phys. Fluids A **2**, 1305 (1990).
[10] A. Gañán-Calvo and J. C. Lasheras, "The dynamics and mixing of small spherical particles in a plane, free shear layer," Phys. Fluids A **3**, 1207 (1990).

[11]H. K. Moffat, "Transport effects associated with turbulence with particular attention to the influence of helicity," Rep. Prog. Phys. **46**, 621 (1983).
[12]M. R. Maxey,, "The motion of small spherical particles in a cellular flow field," Phys. Fluids **30**, 1915 (1987).
[13]M. R. Maxey and S. Corrsin, "Gravitational settling of aerosol particles in randomly oriented cellular flow fields," J. Atmos. Sci. **43**, 1112 (1986).
[14]M. W. Reeks, "Eulerian direct interaction applied to the statistical motion of particles in a turbulent field," J. Fluid Mech. **97**, 569 (1980).
[15]L. P. Wang and D. E. Stock, "Numerical simulation of heavy particle dispersion—Time step and nonlinear drag considerations," ASME J. Fluids Eng. **114**, 100 (1992).
[16]J. R. Rice, *Numerical Methods, Software and Analysis* (McGraw-Hill, New York, 1983).
[17]A. Wolf, J. B Swift, H. L. Swinney, and J. A. Vastano, "Determining Lyapunov exponents from a time series," Physica D **16**, 285 (1985).
[18]F. Varosi, T. M. Antonsen, and E. Ott, "The spectrum of fractal dimensions of passively convected scalar gradients in chaotic fluid flows," Phys. Fluids A **3**, 1017 (1991).
[19]G. I. Taylor, "Diffusion by continuous movements," Proc. R. Soc. London Ser. A **151**, 421 (1921).
[20]G. K. Batchelor and A. A. Townsend, "Turbulent diffusion," *Surveys in Mechanics*, edited by G. K. Batchelor and R. M. Davies (Cambridge U.P., Cambridge, 1956), pp. 352–399.
[21]J. D. Farmer, E. Ott, and J. A. Yorke, "The dimension of chaotic attractors," Physica D **7**, 153 (1983).
[22]J. Kaplan and J. Yorke, *Lecture Notes in Mathematics* (Springer-Verlag, New York, 1979), Vol. 730, p. 204.
[23]H. Aref, "Stochastic particle motion in laminar flows," Phys. Fluids A **3**, 1009 (1991).
[24]C. T. Crowe, R. A. Gore, and T. R. Troutt, "Particle dispersion by coherent structures in free shear flows," Part. Sci. Technol. **3**, 149 (1985).
[25]B. J. Lazaro and J. C. Lasheras, "Particle dispersion in a turbulent, plane shear layer," Phys. Fluids A **1**, 1035 (1989).
[26]J. N. Chung and T. R. Troutt, "Simulations of particle dispersion in an axisymmetric jet," J. Fluid Mech. **186**, 199 (1988).
[27]R. Chein and J. N. Chung, "Simulation of particle dispersion in a two-dimensional mixing layer," AIChE J. **34**, 946 (1988).
[28]L. P. Wang, M. R. Maxey, and R. Mallier, "Structure of stratified shear layer at high Reynolds numbers," submitted to Geophys. Astrophys. Fluid Dyn.
[29]S. Balachandar and M. R. Maxey, "Methods for evaluating fluid velocities in spectral simulations of turbulence," J. Comput. Phys. **83**, 96 (1989).
[30]G. M. Corcos and F. S. Sherman, "The mixing layer: Deterministic models of a turbulent flow. Part 1. Introduction and the two-dimensional flow," J. Fluid Mech. **139**, 29 (1984).
[31]Z. Warhaft, "The interference of thermal fields from line sources in grid turbulence," J. Fluid Mech. **144**, 363 (1984).
[32]B. L. Sawford and J. C. R. Hunt, "Effects of turbulent structure, molecular diffusion and source size on scalar fluctuations in homogeneous turbulence," J. Fluid Mech. **165**, 373 (1986).
[33]D. J. Thomson, "A stochastic model for the motion of particle pairs in isotropic high-Reynolds-number turbulence, and its application to the problem of concentration variance," J. Fluid Mech. **210**, 113 (1990).
[34]G. I. Taylor, "Dispersion of soluble matter in solvent flowing slowly through a tube," Proc. R. Soc. London Ser. A **219**, 186 (1953).